J|A|C|S
ARTICLES
Published on Web 01/30/2003

Is the Ruthenium Analogue of Compound I of Cytochrome P450 an Efficient Oxidant? A Theoretical Investigation of the Methane Hydroxylation Reaction

Pankaz K. Sharma, Sam P. de Visser, François Ogliaro, and Sason Shaik*

Contribution from the Department of Organic Chemistry and the Lise Meitner-Minerva Center for Computational Quantum Chemistry, Hebrew University of Jerusalem, 91904 Jerusalem, Israel

Received August 22, 2002; E-mail: sason@yfaat.ch.huji.ac.il

Abstract: High-valent metal−oxo complexes catalyze C−H bond activation by oxygen insertion, with an efficiency that depends on the identity of the transition metal and its oxidation state. Our study uses density functional calculations and theoretical analysis to derive fundamental factors of catalytic activity, by comparison of a ruthenium−oxo catalyst with its iron−oxo analogue toward methane hydroxylation. The study focuses on the ruthenium analogue of the active species of the enzyme cytochrome P450, which is known to be among the most potent catalysts for C−H activation. The computed reaction pathways reveal one high-spin (HS) and two low-spin (LS) mechanisms, all nascent from the low-lying states of the ruthenium−oxo catalyst (Ogliaro, F.; de Visser, S. P.; Groves, J. T.; Shaik, S. *Angew. Chem. Int. Ed.* **2001**, *40*, 2874−2878). These mechanisms involve a bond activation phase, in which the transition states (TS's) appear as hydrogen abstraction species, followed by a C−O bond making phase, through a rebound of the methyl radical on the metal-hydroxo complex. However, while the HS mechanism has a significant rebound barrier, and hence a long lifetime of the radical intermediate, by contrast, the LS ones are effectively concerted with small barriers to rebound, if at all. Unlike the iron catalyst, the hydroxylation reaction for the ruthenium analogue is expected to follow largely a single-state reactivity on the LS surface, due to a very large rebound barrier of the HS process and to the more efficient spin crossover expected for ruthenium. As such, ruthenium−oxo catalysts (Groves, J. T.; Shalyaev, K.; Lee, J. In *The Porphyrin Handbook*; *Biochemistry and Binding: Activation of Small Molecules*, Vol. 4; Kadish, K. M., Smith, K. M., Guilard, R., Eds.; Academic Press: New York, 2000; pp 17−40) are expected to lead to more stereoselective hydroxylations compared with the corresponding iron−oxo reactions. It is reasoned that the ruthenium−oxo catalyst should have larger turnover numbers compared with the iron−oxo analogue, due to lesser production of suicidal side products that destroy the catalyst (Ortiz de Montellano, P. R.; Beilan, H. S.; Kunze, K. L.; Mico, B. A. *J. Biol. Chem.* **1981**, *256*, 4395−4399). The computations reveal also that the ruthenium complex is more electrophilic than its iron analogue, having lower hydrogen abstraction barriers. These reactivity features of the ruthenium−oxo system are analyzed and *shown to originate from a key fundamental factor, namely, the strong 4d(Ru)-2p(O,N) overlaps, which produce high-lying π^*(Ru−O), σ^*(Ru−O), and σ^*(Ru−N) orbitals* and thereby to lead to a preference of ruthenium for higher-valent oxidation states with higher electrophilicity, for the effectively concerted LS hydroxylation mechanism, and for less suicidal complexes. As such, the ruthenium−oxo species is predicted to be a more robust catalyst than its iron−oxo analogue.

Introduction

High-valent metal−oxo complexes constitute an important family of catalysts that can perform C−H activation by oxygen insertion.[1] Both processes are among the Holy-Grails of chemistry,[1b] and as such, there is a continuing search for efficient catalysts that can perform these actions with high yields, large turnover numbers, and minimal amounts of side products. In parallel, there is also a need for theoretical models, which reveal fundamental factors that govern the catalytic activity of such species.

A unique catalyst for oxygen transfer is the active species of the enzyme cytochrome P450[1f] that can hydroxylate even nonactivated C−H bonds, a feat that can be achieved by only a very few electrophilic reagents from among the huge arsenal available in chemistry. This active species, shown in Figure 1a, comprises the oxo-iron porphyrin, PorFeO, linked to a sixth

(1) (a) For a succinct repertoire of catalyzed C−H activation processes, see: Cornils, B.; Herrmann, W. A.; Schlögl, R.; Wong, C.-H. *Catalysis from A to Z. A Concise Encyclopedia*; Wiley-VCH: Weinheim, Germany, 2000, pp 114−115. (b) Schröder, D.; Schwarz, H. *Angew. Chem., Int. Ed. Engl.* **1995**, *34*, 1973. (c) Groves, J. T.; Shalyaev, K.; Lee, J. In *The Porphyrin Handbook*; Biochemistry and Binding: Activation of Small Molecules, Vol. 4; Kadish, K. M., Smith, K. M., Guilard, R., Eds.; Academic Press: New York, 2000; pp 17−40. (d) *Biomimetic Oxidations Catalyzed by Transition Metal Complexes*; Meunier, B., Ed.; Imperial College Press: London, 1999. (e) Meunier, B.; Bernadou, J. *Struct. Bonding* **2002**, *97*, 1. (f) Ortiz de Montellano, P. R., Ed. *Cytochrome P450: Structures, Mechanism and Biochemistry*, 2nd ed.; Plenum Press: New York, 1995.

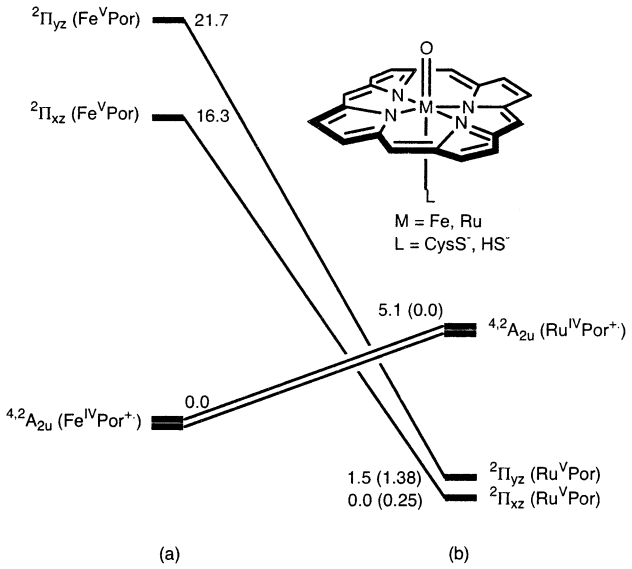

Figure 1. Relative energies (kcal/mol) of lower-lying states of Cpd I(Fe) in (a) and Cpd I(Ru) in (b). The values in parentheses in (b) refer to the situation in a polarizing environment.

ligand, which is a cysteinate, $CysS^-$ moiety. In its stable electromer, this species is called Compound I (Cpd I),[1c−f] a term that denotes a triradicaloid electronic structure possessing an Fe^{IV} center and a porphyrin radical cation situation, hence, $(CysS^-)Por^{+\cdot}Fe^{IV}O$. Due to the catalytic versatility of these natural metalloproteins, a lot of work has been devoted to the preparation of mimetic compounds that can emulate and possibly surpass the efficiency of the iron−oxo species, Cpd I(Fe). One of the key strategies for generating improved synthetic analogues of iron−oxo catalysts is by replacement of the Fe-atom by other neighboring atoms in the periodic table, for example, Mn and Ru,[1−20] and so on. In terms of the general goals stated at the outset, the present work derives fundamental electronic factors that govern the dependence of the catalytic efficiency of Cpd I species on the identity of the transition metal, namely Cpd I(Ru), relative to Cpd I(Fe).

Scheme 1. Schematic Representation of Methane Hydroxylation by the Ru Analogue of Cpd I

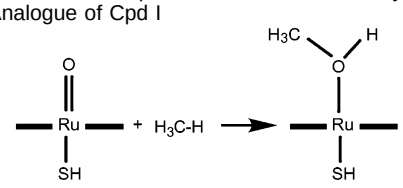

Experimentally, $PorRu^{IV}O$ derivatives without the sixth ligand are well-known to be inactive[1c] as catalysts. Their behavior is analogous to that of the one-electron-reduced iron species, $(L)PorFe^{IV}O$, which are known to be poor electrophiles. Dioxo Ru^{VI}−porphyrin systems were reported to catalyze asymmetric epoxidation of terminal and trans-disubstituted olefins and to display some enantiomeric selectivity in kinetic resolution of secondary alcohols, and apparently, hydroxylation of tertiary alkanes.[6] Aerobic epoxidation of olefins by Ru−porphyrin catalysts was reported as well, and was postulated to be catalyzed by Ru^{VI}−dioxo species, formed via the disproportionation of Ru^{IV}−O species.[20] Thus, initially it was thought that the active species in ruthenium catalysts was the dioxo Ru^{VI}−porphyrin complex. However, it has become evident[1c] that the more active form of the ruthenium catalyst is, in fact, the species $(L)PorRu^VO$. Indeed, Ru^V−oxo catalysts are well known to have a variety of macrocyclic ligands.[11] However, the putative active species with porphyrin, $(L)PorRu^VO$, has not been isolated, nor has it ever been characterized by any physical means.

Recently, we used density functional theoretical (DFT) calculations to compare the ruthenium and iron Cpd I species, Cpd I(Ru) and Cpd I(Fe).[21] The results, summarized in Figure 1, show that in the gas phase with a thiolate ligand, the ground state is indeed $(HS)PorRu^VO$. However, in a polarizing environment, it exists most likely in equilibrium with the $(HS)Por^{+\cdot}Ru^{IV}O$ state.[21] Irrespective of the conditions, it is apparent that the states of Cpd I(Fe) and Cpd I(Ru) are very different. Thus, while in Cpd I(Fe), the ground state is the $^{4,2}A_{2u}$ type $(HS)Por^{+\cdot}Fe^{IV}O$, in Cpd I(Ru), there are two low-lying $^2\Pi_{xz}$ and $^2\Pi_{yz}$ states of the $(L)PorRu^VO$ variety, which are either the ground states (in the gas phase) or in close equilibrium with the $^{4,2}A_{2u}$ states in a solvent environment (with a dielectric constant, $\epsilon = 5.7$). Due to this difference, it was postulated[21] that the ruthenium−oxo species will be more electrophilic than the iron−oxo species, in accord with preliminary observations.[1c,22] While the computed differences in the states of Cpd I(Fe) and Cpd I(Ru) suggest that these species might exhibit different reactivity patterns, this supposition requires computational vindication and theoretical foundation. In light of this necessity, our aims in the present work are to elucidate the key factors that determine the C−H bond activation and hydroxylation efficiency of Cpd I(Ru) versus those of Cpd I(Fe).

Toward these aims, we studied the mechanism of a model alkane hydroxylation by Cpd I(Ru). As depicted in Scheme 1, methane served as the model alkane, porphine was used as the macrocycle, and thiolate (HS^-) was chosen as the sixth ligand. These choices were made to enable us to compare, on equal

(2) Zhang, J.-L.; Che, C.-M. *Org. Lett.* **2002**, *4*, 1911−1914.
(3) Dunn, A. R.; Dmochowski, I. J.; Bilwes, A. M.; Gray, H. B.; Crane, B. R. *Proc. Natl. Acad. Sci. U.S.A.* **2001**, *98*, 12420−12425.
(4) Dijksman, A.; Marino-González, A.; Mairata i Payeras, A.; Arends, I. W. C. E.; Sheldon, R. A. *J. Am. Chem. Soc.* **2001**, *123*, 6826−6833.
(5) (a) Leuenberger, M. G.; Engeloch-Jarret, C.; Woggon, W.-D. *Angew. Chem., Int. Ed.* **2001**, *40*, 2613−2617. (b) French, R. R.; Holzer, P.; Leuenberger, M. G.; Woggon, W.-D. *Angew. Chem., Int. Ed.* **2000**, *39*, 1267−1269.
(6) (a) Gross, Z.; Ini, S. *Inorg. Chem.* **1999**, *38*, 1446−1449. (b) Gross, Z.; Ini, S. *Org. Lett.* **1999**, *1*, 2077−2080.
(7) Groves, J. T.; Bonchio, M.; Carofiglio, T.; Shalyaev, K. *J. Am. Chem. Soc.* **1996**, *118*, 8961−62.
(8) Fackler, N. L. P.; Zhang, S.; O'Halloran, T. V. *J. Am. Chem. Soc.* **1996**, *118*, 481−482.
(9) Groves, J. T.; Roman, J. S. *J. Am. Chem. Soc.* **1995**, *117*, 5594−5595.
(10) Bakke, J. M.; Bethell, D. *Acta Chem. Scand.* **1992**, *46*, 644−649.
(11) Che, C.-M.; Ho, C.; Lau, T.-C. *J. Chem. Soc., Dalton Trans.* **1991**, 1259−1263.
(12) Dengel, A. C.; Griffith, W. P. *Inorg. Chem.* **1991**, *30*, 869−871.
(13) Che, C.-M.; Yam, V. W.-W.; Mak, T. C. W. *J. Am. Chem. Soc.* **1990**, *112*, 2284−2291.
(14) Dengel, A. C.; Griffith, W. P.; O'Mahoney, C. A.; Williams, D. J. *J. Chem. Soc., Chem. Commun.* **1989**, 1720−1721.
(15) Groves, J. T.; Ahn, K.-H., Quinn, R. *J. Am. Chem. Soc.* **1988**, *110*, 4217−4220.
(16) Che, C.-M.; Lai, T.-F.; Wong, K.-Y. *Inorg. Chem.* **1987**, *26*, 2289−2299.
(17) Che, C.-M.; Wong, K.-Y. *J. Chem. Soc., Chem. Commun.* **1986**, 229−230.
(18) Mak, T. C. W.; Che, C.-M.; Wong, K.-Y. *J. Chem. Soc., Chem. Commun.* **1985**, 986−988.
(19) Che, C.-M.; Wong, K.-Y.; Mak, T. C. W. *J. Chem. Soc., Chem. Commun.* **1985**, 8−10.
(20) Groves, J. T.; Quinn, R. J. *J. Am. Chem. Soc.* **1985**, *107*, 5790−5792.
(21) Ogliaro, F.; de Visser, S. P.; Groves, J. T.; Shaik, S. *Angew. Chem., Int. Ed.* **2001**, *40*, 2874−2878.
(22) Groves, J. T. Preliminary data presented at the ICPP-1 Symposium, Dijon, July, 2000.

footing, the reactivity patterns of Cpd I(Ru) to those revealed for Cpd I(Fe) in our previous study of methane hydroxylation.[23a]

Methods

The computational procedures followed procedures established in previous publications.[21,23] This study was carried out with DFT. Calculations were done with the Jaguar 4.1 package[24] using the unrestricted HF-DFT[25] hybrid (UDFT) functional, B3LYP.[26] A double-ζ quality basis set was used, employing 6-31G for C, H, N, S, and O, and LACVP,[27] coupled with the Los Alamos effective core potential for Ru. This basis set, LACVP(6-31G), has been proven qualitatively reliable and found to be similar in performance to higher-level basis sets. Frequency analyses of the fully converged Jaguar structures were carried out with the Gaussian98 suite of programs,[28] which has the facility to compute vibrational frequencies analytically and is faster in this respect than Jaguar.

To explore the potential energy surfaces, for critical species, we ran geometry scans using one degree of freedom as a reaction coordinate. For instance, starting with ^{4}**2** (see Scheme 3), the O−H bond was stretched stepwise until its dissociation took place. The highest point of this scan was then used as the starting point to locate the transition-state structure along that mode. Similar procedures were applied to all other species (see Supporting Information).

Results

The layout of the Results section is as follows: we start with a discussion of the critical orbitals relevant to this reaction process. We then summarize the important low-lying states of the reactant (HSPorRuO) and so forth, which will be followed by the various critical species in different electronic states involved at each of the reaction steps.

The Critical Orbitals. Let us begin with a cursory look at the key orbitals involved in this reaction, shown in Scheme 2. These are the five metal d-orbitals and the a_{2u} orbital of porphine. The d-block orbitals are (a) the $d_{x^2-y^2}$ orbital that lies in the plane of the porphyrin ring, designated d_δ, (b) two orbitals of the type π^*_{RuO} which are π^*_{xz} or π^*_{yz}. These π^* orbitals are sometimes referred to as d_π. In Ru^{IV} and Ru^{V} these orbitals are generally occupied. In addition, there are vacant orbitals: the metal d_{z^2} (σ^*) orbital, which is antibonding in the S−Ru−O axis, and the metal d_{xy}(σ^*) orbital that is antibonding across the Ru−N bonds of the ruthenium porphine base. The a_{2u} orbital, on the right-hand side, is mixed with the p_z orbital on the sulfur atom. Similarly, the π^*_{yz} orbital mixes with the corresponding p_y orbital on sulfur, and is therefore slightly higher than π^*_{xz}.

Scheme 2. Frontier Orbitals of Metal−Oxo Species; Their Occupancies in the $^{4,2}A_{2U}$ and $^2\Pi_{xz,yz}$ States Are Specified in the Box

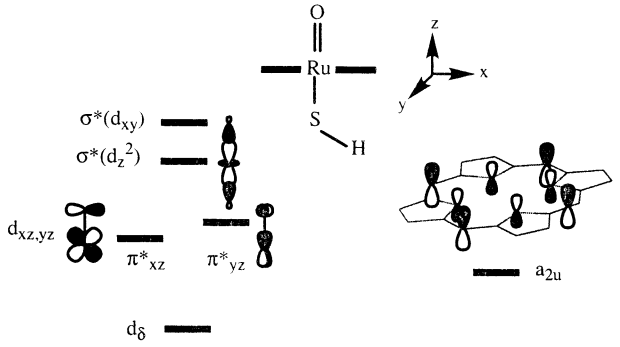

$^{4,2}A_{2u} : d_\delta^2 \pi^*_{xz}{}^1 \pi^*_{yz}{}^1 a_{2u}{}^1$

$^2\Pi_{xz} : d_\delta^2 \pi^*_{xz}{}^1 a_{2u}{}^2$

$^2\Pi_{yz} : d_\delta^2 \pi^*_{yz}{}^1 a_{2u}{}^2$

As already shown in Figure 1b above, our previous study[21] revealed a few closely lying states, which differ in the occupancy of these orbitals. The $^{4,2}A_{2u}$ states involve Ru^{IV} with three singly occupied orbitals: the two π^* type and the a_{2u}. Ferromagnetic and antiferromagnetic coupling of these three electrons give rise to the quartet and doublet A_{2u} states. In the Ru^{V} situation, one of the π^* electrons is shifted to the a_{2u} orbital, thus giving rise to the two doublet states: $^2\Pi_{xz}$ and $^2\Pi_{yz}$, with one electron in the π^*_{xz} or π^*_{yz} orbital. Since π^*_{yz} is slightly higher in energy than π^*_{xz}, the lower state is $^2\Pi_{xz}$. As shown before,[21] medium polarization condenses the A_{2u} and Π states into an energy range of 1.5 kcal/mol. The $\Pi-A_{2u}$ gap will depend, however, on the nature of the axial ligand.[21] Thiolates, which are good electron donors, are known to raise the a_{2u} orbital[29] and thereby stabilize the A_{2u} states, which involve single occupancy in this orbital. Ligands that are poorer electron donors, such as H_2O and so forth, will not stabilize the A_{2u} states and are therefore expected to possess $^2\Pi_{xz,yz}$ ground states even when medium polarization effect is included.

The Reaction Sequence. As revealed by the calculations, methane oxygenation by Cpd I(Ru) takes place in a sequence of the steps depicted in Scheme 3. Initial hydrogen abstraction from the long-range complex (**1**) leads to the intermediate, HSPorRuO−H- - -CH_3• (**2**), which upon reorientation of the CH_3 group is transformed to the rebound cluster (**3**). The latter then undergoes C−O bond formation and generates **4**, (HS)-PorRu(H_3C−O−H), the alcohol product complex. This sequence of reaction steps has already been studied in detail and

(23) (a) Ogliaro, F.; Harris, N.; Cohen, S.; Filatov, M.; de Visser, S. P.; Shaik, S. *J. Am. Chem. Soc.* **2000**, *122*, 8977−8989. (b) de Visser, S. P.; Ogliaro, F.; Harris, N.; Shaik, S. *J. Am. Chem. Soc.* **2001**, *123*, 3037−3047. (c) Ogliaro, F.; de Visser, S. P.; Cohen, S.; Kaneti, J.; Shaik, S. *ChemBioChem* **2001**, *11*, 848−851.
(24) Jaguar 4.1; Schrödinger, Inc.: Portland, OR, 1991−2000.
(25) (a) Hohenberg, P.; Kohn, W. *Phys. Rev. B* **1964**, *136*, 864. (b) Kohn, W.; Sham, L. *Phys. Rev. A* **1965**, *140*, 1133. (c) Parr, R. G.; Yang, W. *Density-Functional Theory of Atoms and Molecules*; Oxford: New York, 1989.
(26) (a) Becke, A. D.; *J. Chem. Phys.* **1993**, *98*, 5648−5652; **1992**, *96*, 2155−2160; **1992**, *97*, 9173−9177. (b) Lee, C.; Yang, W.; Parr, R. G. *Phys. Rev. B.* **1988**, *37*, 785.
(27) Hay, J. P.; Wadt, W. R. *J. Chem. Phys.* **1985**, *82*, 270−283, 284−298, 299−308.
(28) Frisch, M. J.; Trucks, G. W.; Schlegel, H. B.; Scuseria, G. E.; Robb, M. A.; Cheeseman, J. R.; Zakrzewski, V. G.; Montgomery, J. A., Jr.; Stratmann, R. E.; Burant, J. C.; Dapprich, S.; Millam, J. M.; Daniels, A. D.; Kudin, K. N.; M. C. Strain, M. C.; Farkas, O.; Tomasi, J.; Barone, V.; Cossi, M.; Cammi, R.; Mennucci, B.; Pomelli, C.; Adamo, C.; Clifford, S.; Ochterski, J.; Petersson, G. A.; Ayala, P. Y.; Cui, Q.; Morokuma, K.; Malick, D. K.; Rabuck, A. D.; Raghavachari, K.; Foresman, J. B.; Cioslowski, J.; Ortiz, J. V.; Baboul, A. G.; Stefanov, B. B.; G. Liu, G.; Liashenko, A.; Piskorz, P.; Komaromi, I.; Gomperts, R.; Martin, R. L.; Fox, D. J.; Keith, T.; Al-Laham, M. A.; Peng, C. Y.; Nanayakkara, A.; Gonzalez, C.; Challacombe, M.; Gill, P. M. W.; Johnson, B.; Chen, W.; Wong, M. W.; Andres, J. L.; Gonzalez, C.; Head-Gordon, M.; Replogie, E. S.; Pople, J. A. *Gaussian 98*; Gaussian, Inc.: Pittsburgh, PA, 1998.
(29) (a) Loew, G. H.; Kert, C. J.; Hjelmeland, L. M.; Kirchner, R. F. *J. Am. Chem. Soc.* **1977**, *99*, 3534−3536. (b) Hanson, L. K.; Chang, C. K.; Davis, M. S.; Fajer, J. *J. Am. Chem. Soc.* **1981**, *103*, 663−670. (c) de Visser, S. P.; Ogliaro, F.; Gross, Z.; Shaik, S. *Chem. Eur. J.* **2001**, *7*, 4954−4960. (d) Green, M. T. *J. Am. Chem. Soc.* **1998**, *120*, 10772−10773. (e) Ohta, T.; Matsuura, K.; Yoshizawa, K.; Morishima, I. *J. Inorg. Biochem.* **2000**, *82*, 141−152. (f) Yoshizawa, K.; Kagawa, Y.; Shiota, Y. *J. Phys. Chem. B.* **2000**, *104*, 12365−12370. (g) Harris, D. L. *Curr. Opin. Chem. Biol.* **2001**, *5*, 724−735.

Scheme 3. Various Steps of the Methane Hydroxylation Reaction by Cpd I(Ru)

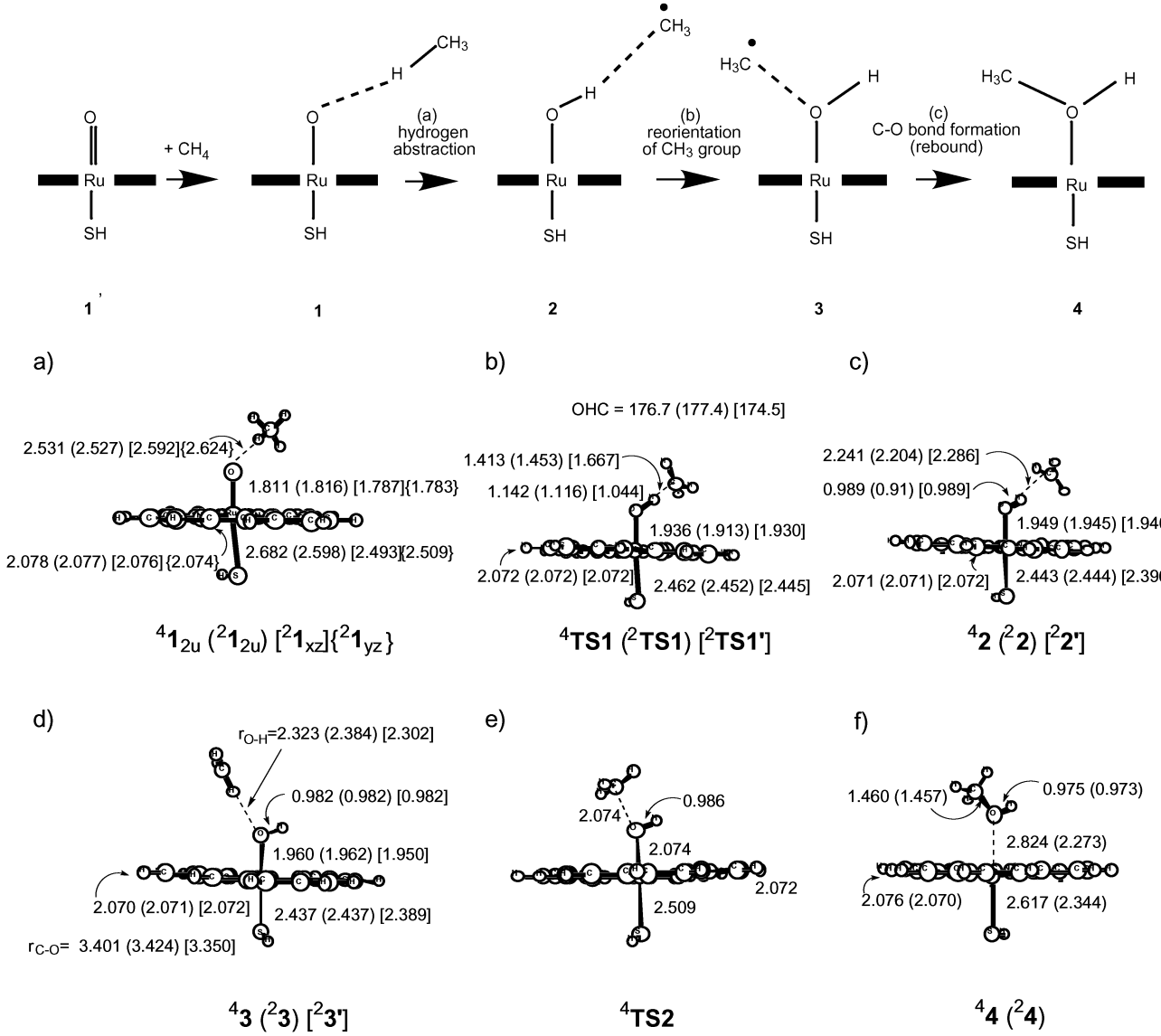

Figure 2. Key geometric parameters of the species involved in this study.

established for the Cpd I(Fe).[23a,b,30] Furthermore, Cpd I(Fe) is a two-state reagent since it has two closely lying states, $^2A_{2u}$ and $^4A_{2u}$. Consequently, all the species appear in the two spin-varieties, and the mechanistic information is a two-state content. This scenario has been termed two-state reactivity (TSR).[23a,b,30−32] In the present case of Cpd I(Ru), we might suspect a more complex situation due to the proximity of the $^{2,4}A_{2u}$ and the $^2\Pi_{xz,yz}$ states. As shall be seen later, however, the situation is considerably simpler compared with that of the iron case.

The Reactant Cluster. On the basis of our earlier study,[21] the present investigation begins with the four low-lying states of Cpd I(Ru). Upon interaction with methane these four states form long-range clusters (**1**), which are depicted in Figure 2a, and are distinguished by using the corresponding state indicator as a subscript. The interaction energies are small, 2−3 kcal/mol (see Figure 5 later), but larger than those in the corresponding Cpd I(Fe)/CH_4 clusters.[23a]

The relative ordering of the Cpd I(Ru)/CH_4 clusters is similar to the corresponding state ordering in Cpd I(Ru) in the gas phase.[21] All the reactant clusters, ^{4,2}**1**, are seen to have a loose coordination between Cpd I and methane with O- - -H distances of ca. 2.53−2.62 Å. The $^2\mathbf{1}_{xz}$ state is seen to possess shorter Ru−O and Ru−S bonds compared to those in the $^{4,2}\mathbf{1}_{2u}$ states. This trend is accounted for by the electron occupancy in the π^* orbitals (Scheme 2). Thus, the $^{4,2}\mathbf{1}_{2u}$ species, which possess two electrons in these orbitals, have longer Ru−O and Ru−S bonds. By contrast, the $^2\Pi$ states, in which one of these orbitals is vacant, have shorter Fe−O and Fe−S bonds.

The Reaction Intermediates. The hydrogen abstraction step terminates at the radical intermediates, labeled **2** in Figure 2c. The hydrogen abstraction is attended by a formal electron shift

(30) (a) Filatov, M.; Harris, N.; Shaik, S. *Angew. Chem., Int. Ed*. **1999**, *38*, 3510−3512. (b) Yoshizawa, K.; Kamachi, T.; Shiota, Y. *J. Am. Chem. Soc.* **2001**, *123*, 9806−9816. (c) de Visser, S. P.; Ogliaro, F.; Sharma, P. K.; Shaik, S. *Angew. Chem., Int. Ed.* **2002**, *41*, 1947−1951. (d) de Visser, S. P.; Ogliaro, F.; Sharma, P. K.; Shaik, S. *J. Am. Chem. Soc*. **2002**, *124*, 11809−11826.

(31) (a) Shaik, S.; Filatov, M.; Schröder, D.; Schwarz, H. *Chem. Eur. J.* **1998**, *4*, 193−199. (b) Schröder, D.; Shaik, S.; Schwarz, H. *Acc. Chem. Res.* **2000**, *33*, 139−145. (c) Shaik, S.; de Visser, S. P.; Ogliaro, F.; Schwarz, H.; Schröder, D. *Curr. Opin. Chem. Biol.* **2002**, *6*, 556−567.

(32) For a recent study of the two-state reactivity of manganese salen, see: Linde, c.; Koliaï, N.; Norrby, P.-O.; Åkermark, B. *Chem. Eur. J.* **2002**, *8*, 2568−2573.

Scheme 4. Depiction of the Electron Reorganization in the Frontier Orbitals Involved in the Hydrogen Abstraction Step

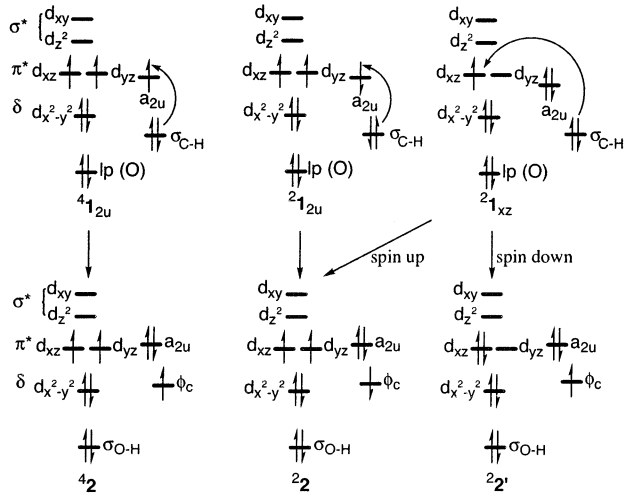

from the C−H bond orbital into the empty, or singly occupied, orbital of the ruthenium−oxo porphyrin moiety.

Scheme 4 shows these formal electron shifts. A shift of a spin-down electron, in $^4\mathbf{1}_{2u}$, leads to the intermediate $^4\mathbf{2}$ that possesses singly occupied π^* orbitals and ϕ_C, the latter being the orbital of the methyl radical. Similarly, a shift of a spin-up electron starting from $^2\mathbf{1}_{2u}$ leads to the intermediate state, $^2\mathbf{2}$. The same state is obtained by shifting a spin-up electron from $^2\mathbf{1}_{xz}$ to the π^* (d_{yz}) orbital. On the other hand, shifting a spin-down electron within $^2\mathbf{1}_{xz}$ leads to $^2\mathbf{2}'$. In this latter state, the π^* electrons are singlet-paired, and its energy is, therefore, higher than that of $^2\mathbf{2}$. Another doublet cluster intermediate ($^2\mathbf{2}''$) with antiferromagnetic coupling of the unpaired electrons on the π^*_{xz} and π^*_{yz} orbitals was found to lie 0.2 kcal/mol higher above $^2\mathbf{2}'$. Similarly, shifting an electron within $^2\mathbf{1}_{2u}$ to the π^* instead of the a_{2u} orbital led to a higher-energy species of the Ru^{III} variety. These Ru^{III} intermediates were not studied further, since no bond activation transition state could be located which connected the clusters, **1**, to these intermediates. The $^2\mathbf{1}_{yz}$ cluster gives precisely the same intermediate states, which are, therefore, not shown explicitly in Scheme 4. Clearly, the preference of ruthenium for the higher-valent situations carries over from Cpd I(Ru)[21] to the intermediate. Thus, in all the lower-lying intermediates the ruthenium has a formal oxidation state of Ru^{IV} with a d^4 electronic configuration in the d-block. This is in contrast to the corresponding iron intermediates, which appeared in oxidation states of Fe^{IV} and Fe^{III}.[23a,b] The geometric characteristics of $^{2,4}\mathbf{2}$ and $^2\mathbf{2}'$ are given in Figure 2c. They look quite similar with the exception of the OH- - -C and O−H distances which are the shortest for $^2\mathbf{2}$.

H-Abstraction Transition States. Unlike the case of hydrogen abstraction by Cpd I(Fe), where only two low-lying transition states (TS's) were characterized, here we found three low-lying hydrogen abstraction TS's. These species, which are depicted in Figure 2b, show stretching of the C−H bond and formation of the O−H bond. The C−H bond is highly stretched but less so than in the corresponding iron species.[23a] An exception is ^{2}**TS1′** for which the C−H bond is very long, and can be considered to lie "late" on the reaction coordinate in comparison with the other two species. The ∠OHC angle in all the TS's is virtually linear, thereby further supporting the nature of the TS's as hydrogen abstraction species. Another indication of this nature is projected from the imaginary mode of these TS's in Figure 3. With the exception of ^{2}**TS1′**, this mode has a high imaginary frequency that is indicative of hydrogen abstraction. For ^{2}**TS1′** the frequency is low in accord with the very "late" nature of this TS.

Geometry scans (see Supporting Information) starting from ^{2}**TS1** and ^{2}**TS1′** correlated down to the most stable cluster, $^2\mathbf{1}_{xz}$. However, when the scan started from $^2\mathbf{1}_{2u}$, it also passed via ^{2}**TS1**. This suggests that ^{2}**TS1** bifurcates to $^2\mathbf{1}_{xz}$ and $^2\mathbf{1}_{2u}$, and perhaps also to $^2\mathbf{1}_{yz}$. Later on we shall rationalize the finding of only three and not four low-lying TS's.

Rebound Clusters. The rebound cluster, **3** (Figure 2d), is an intermediate in which the CH_3 moiety forms a CH- - -O interaction, and occupies a rebound position about the ruthenium−hydroxo species. It is seen that the H- - -O distances, of 2.323 Å (^{4}**3**), 2.384 Å (^{2}**3**), and 2.302 Å (^{2}**3′**), respectively, are well within an acceptable range for CH- -O hydrogen bond. The barrier for the formation of the quartet rebound cluster (^{4}**3**) from its cluster intermediate (^{4}**2**) is quite low, of the order of 0.7 kcal/mol. The corresponding values for ^{2}**3** and ^{2}**3′** are similar and small, also at 0.4 kcal/mol for each of these states. Such hydrogen-bonded species may not remain intermediates in solution. In the rebound mechanisms of Cpd I(Fe) these species are not real intermediates.[23a, 30d]

Rebound Transition State. Only one rebound transition state could be located. This is ^{4}**TS2** for the high-spin quartet surface. As can be seen from Figure 2e, ^{4}**TS2** has longer Ru−O and Ru−S bonds, compared with those in the rebound intermediate, ^{4}**3**. This bond lengthening is associated with a true chemical barrier in perfect analogy to the behavior of the iron system.[23a] The reaction vector of ^{4}**TS2** is shown in Figure 3 and is seen to correspond to C−O bond making.

In contrast to the high-spin rebound, the two corresponding low-spin processes were found to proceed from the CH- - -O bonded species (^{2}**3**, ^{2}**3′**) to the alcohol complexes in a barrierless fashion. While the scans for either of these two pathways apparently indicated the presence of a potential barrier, the search for the transition state always ended up with minimum-energy structures instead. This deceptive appearance of a potential barrier is caused by the rotation of the CH_3 group of the rebound cluster around the Ru−O bond, from one CH- - -O bond to another, and not by the C−O bond making. This process, which seems to follow a topsy-turvy potential energy surface, gives the impression of the existence of a potential barrier. In fact, allowing the C−H bond to deviate from the hydrogen bond axis results in a descent toward the doublet alcohol product.

The existence of ^{4}**TS2** for the high-spin pathway and the absence of a **TS** on the alternative, low-spin surface can be rationalized as before,[23a,30a,c,d,31c] in terms of the orbitals involved in electron promotion during this step. Thus, for the high-spin path, an electron from the $CH_3^\bullet$ radical is promoted to the d_{z^2}-(σ^*) orbital of the Ru atom (Scheme 5), which is high-lying, and hence, a barrier has to be traversed to accommodate this electronic promotion. This is also reflected in the longer Ru−O and Ru−S bond lengths in ^{4}**TS2** compared to those in ^{4}**3** (Figure 2d,e). On the other hand, the orbital to which the electron is promoted for the low-spin route is a low-lying $d_{xz,yz}(\pi^*)$ orbital, and hence, no such barrier is encountered in this pathway.[23a]

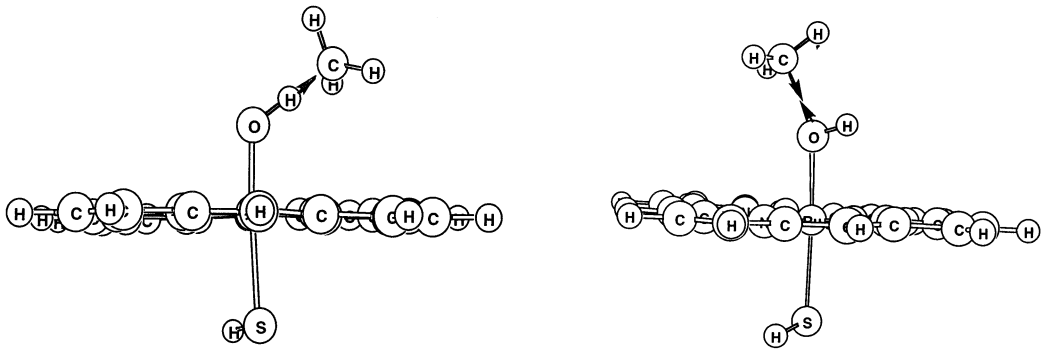

^{4}**TS1** ω_i = i1382 cm^{-1}
^{2}**TS1** ω_i = i1041 cm^{-1}
^{2}**TS1'** ω_i = i185 cm^{-1}

^{4}**TS2** ω_i = i570 cm^{-1}

Figure 3. Imaginary modes and their frequencies in the three hydrogen abstraction transition states (left) and the high-spin rebound transition state (right).

Scheme 5. Depiction of the Electron Reorganization in the Frontier Orbitals Involved in the Rebound Step

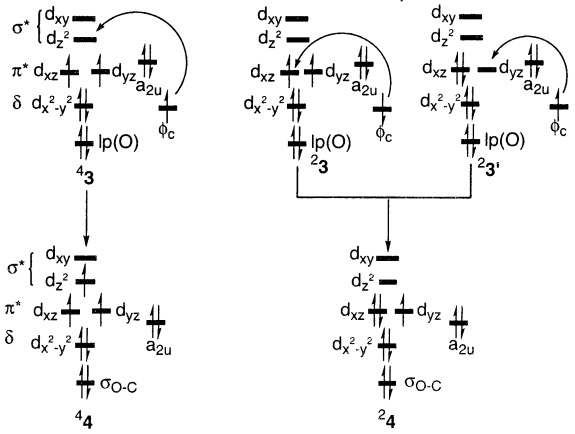

Products. The product complex involving CH_3OH ligated to Ru is formed in the final step. The most interesting feature of this step is the virtual detachment of the alcohol from the ruthenium−porphine moiety in the quartet state, ^{4}**4** (see Figure 2f; Ru−O bond length is 2.824 Å), while for the doublet state, ^{2}**4**, no such detachments were observed (Ru−O bond length is 2.273 Å). This observation can be reasoned out in terms of the orbital involved in the reorganization that takes place during the product formation step, as depicted in Scheme 5. In the case of ^{4}**4**, it is the antibonding $d_{z^2}(\sigma^*)$ orbital that gets populated by shifting an electron from the $CH_3^\bullet$ radical during this step. This orbital, shown in Scheme 2, involves Ru−O and Ru−S antibonding interactions. As such, population of this orbital results in elongation of the Ru−S and Ru−O bonds and in the snapping off of the CH_3OH unit altogether. For ^{2}**4**, however, a similar situation does not arise. Here, the electron is transferred to one of the π^* orbitals of Ru, d_{xz} that is lower-lying and which does not give rise to unfavorable interaction of the kind observed for ^{4}**4**. Interestingly, due to the detachment of methanol, the high-spin reaction pathway is almost thermoneutral (see later in Figure 4), whereas the low-spin pathway is highly exothermic. This energy splitting of the high-spin and low-spin products is considerably larger than that found for the iron case.[23a] This difference originates from the stronger 4d−2p(O) overlap in Ru compared with the 3d−2p(O) overlap in Fe, as a result of which the d-block orbitals are higher-lying in Ru complexes in comparison to those in Fe complexes.[21] Thus, the $d_{z^2}(\sigma^*)$ is sufficiently high in energy (see later Scheme 7) so that its population in ^{4}**4** leads virtually to a loss of one ligand.

Table 1. Atomic/Group Spin Density Values of the Various Species Involved in the Methane Hydroxylation Reaction by the Ru Analogue of Cpd I

	Ru	O	H	SH	CH_3	Por
^{4}**1**$_{2u}$ ($\pi^*_{xz}\uparrow\pi^*_{yz}\uparrow a_{2u}\uparrow$)	0.92	1.01	0.00	0.52	0.00	0.55
^{4}**TS1**[a]	1.19	0.73	−0.05	0.35	0.64	0.14
^{4}**2** ($\pi^*_{xz}\uparrow\pi^*_{yz}\uparrow a_{2u}\uparrow\downarrow\phi\uparrow$)	1.28	0.37	0.01	0.31	0.95	0.08
^{2}**1**$_{xz}$ ($\pi^*_{xz}\uparrow\pi^*_{yz}{}^0 a_{2u}\uparrow\downarrow$)	0.61	0.84	0.00	−0.35	0.00	−0.10
^{2}**TS1′**[b]	0.12	0.47	−0.04	−0.37	0.78	0.04
^{2}**2′** ($\pi^*_{xz}\uparrow\downarrow\pi^*_{yz}{}^0 a_{2u}\uparrow\downarrow\phi\uparrow$)[c]	0.09	0.03	0.01	−0.05	0.95	−0.03
^{2}**1**$_{2u}$ ($\pi^*_{xz}\uparrow\pi^*_{yz}\uparrow a_{2u}\downarrow$)	0.86	0.93	0.00	−0.37	0.00	−0.42
^{2}**TS1**[b]	1.24	0.05	0.08	0.25	−0.63	0.01
^{2}**2** ($\pi^*_{xz}\uparrow\pi^*_{yz}\uparrow a_{2u}\uparrow\downarrow\phi\downarrow$)	1.28	0.30	−0.01	0.30	−0.94	0.07
^{4}**3** ($\pi^*_{xz}\uparrow\pi^*_{yz}\uparrow a_{2u}\uparrow\downarrow\phi\uparrow$)	1.30	0.30	0.00	0.32	1.00	0.08
^{4}**TS2** ($\sigma^*_{z^2}\uparrow\pi^*_{xz}\uparrow\pi^*_{yz}\uparrow a_{2u}\uparrow\downarrow$)	1.70	0.05	0.02	0.43	0.68	0.12
^{4}**4** ($\sigma^*_{z^2}\uparrow\pi^*_{xz}\uparrow\pi^*_{yz}\uparrow a_{2u}\uparrow\downarrow$)	2.24	0.01	0.00	0.45	0.01	0.20
^{2}**3′** ($\pi^*_{xz}\uparrow\downarrow\pi^*_{yz}{}^0 a_{2u}\uparrow\downarrow\phi\uparrow$)	−0.09	−0.01	0.00	0.07	1.00	0.03
^{2}**3** ($\pi^*_{xz}\uparrow\pi^*_{yz}\uparrow a_{2u}\uparrow\downarrow\phi\downarrow$)	1.29	0.30	0.00	0.30	−0.99	0.10
^{2}**4** ($\pi^*_{xz}\uparrow\downarrow\pi^*_{yz}\uparrow a_{2u}\uparrow\downarrow$)	0.72	0.00	0.00	0.24	0.00	0.04

[a] The amount of charge transferred from CH_4 to the ruthenium−oxo complex (Q_{CT}) is −0.32. [b] Q_{CT}(^{2}**TS1′**) = −0.40; Q_{CT}(^{2}**TS1**) = −0.23. [c] The antiferromagnetic ^{2}**2″** state with ($\pi^*_{xz}\uparrow\pi^*_{yz}\downarrow a_{2u}\uparrow\downarrow\phi\uparrow$) is 0.2 kcal/mol higher.

Discussion

Electronic Structure of the Key Species. Table 1 summarizes the orbital occupation of the various critical species, as deduced from their natural orbital analysis, and also provides their spin density distribution based on Mulliken population analysis. The orbital labels in the table follow Schemes 2, 4, and 5.

The orbitals of the hydrogen abstraction transition states are not specified in the table, since the singly occupied ones have mixed character that requires some elucidation. The spin density distribution of these transition states is quite unique, and Scheme 6 compares it to the corresponding spin distribution in the iron transition states, called ^{4,2}**TS$_H$**.[23a] Thus, while for iron the significant spin density on porphine reveals the $^{4,2}A_{2u}$ parenthood of the TS's, in the ruthenium species, the porphine spin density

Scheme 6. Comparison of the Spin Density Distribution in Transition States for the C−H Bond Activation Step by Cpd I(Ru) and Cpd I(Fe)

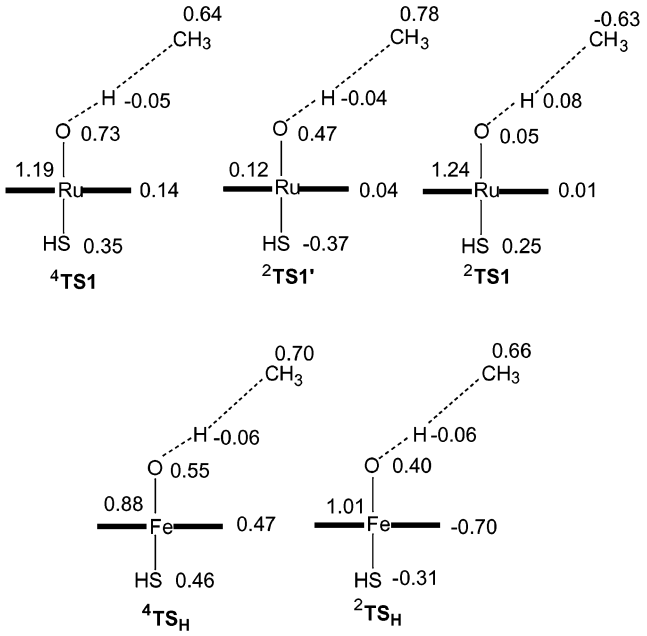

is close to zero. This suggests that in all the ruthenium species the a_{2u} orbital is filled, whereas in the iron species the a_{2u} orbital is singly occupied. The natural orbital analysis supports this suggestion and reveals a doubly occupied a_{2u}-type orbital. All attempts to locate transition states with single occupation in this a_{2u}-type orbital, by swapping the orbitals of the **^{4,2}TS1** and **^{2}TS1′** species, resulted in much higher-energy species that fell back into **^{4,2}TS1** and **^{2}TS1′**.

The reason for this difference between iron and ruthenium originates in the overlap capabilities of the metal 4d and the 3d orbitals with the oxygen 2p orbitals.[21] A weaker 3d(Fe)−2p(O) overlap generates low-lying π^* orbitals, and consequently, the Fe^{III} states with single occupancy in a_{2u} are low-lying; in the case of methane hydroxylation they are the lowest-energy TS's,[23a] as shown in Scheme 6. In contrast, the stronger 4d(Ru)−2p(O) overlap generates high-lying π^* orbitals, and therefore, the a_{2u} orbitals of **^{2,4}TS1** and **^{2}TS1′** become doubly occupied at the expense of π^*.

Still, the spin densities on the metal in the ruthenium species in Scheme 6 are a bit odd. In two of the species, **^{4}TS1** and **^{2}TS1**, Ru has a spin density slightly more than unity, while in the third species, **^{2}TS1′**, the Ru spin density is negligible. In **^{4}TS1,** the RuO moiety carries approximately two spins corresponding to a $\delta^2 \pi^{*1}_{xz} \pi^{*1}_{yz}$ d-block configuration, which can be associated with the Ru^{IV} oxidation state. However, in the other TS species the spin densities do not correspond to any easily conceivable oxidation state of ruthenium. To elucidate the electronic structures of the TS's, we investigated the natural orbitals in detail with an attempt to construct an orbital picture for the TS's.

Figure 4 is such an orbital mixing diagram that generates the key frontier orbitals of the TS's from the fragment orbitals of the ruthenium−oxo species and the σ and σ^* orbitals of the stretched C−H bond that undergoes activation. On the left-hand side (in the box) we show the a_{2u} and π^*_{xz} orbitals, which carry three electrons in all the TS's species. The singly occupied π^*_{xz} orbital is the one which is orthogonal to the plane of the Ru−O−H−C moiety in the TS, while the a_{2u} is kept doubly filled in keeping with its lower energy relative to that of the π^* orbitals.[21] The orbitals that are involved in the mixing with the H−C orbitals are the doubly filled π_{yz} and the vacant π^*_{yz}. With this initial occupancy, the ruthenium−oxo porphine moiety has the nature of the $^2\Pi_{xz}$ state (Figure 1b), which is the ground state of Cpd I(Ru).

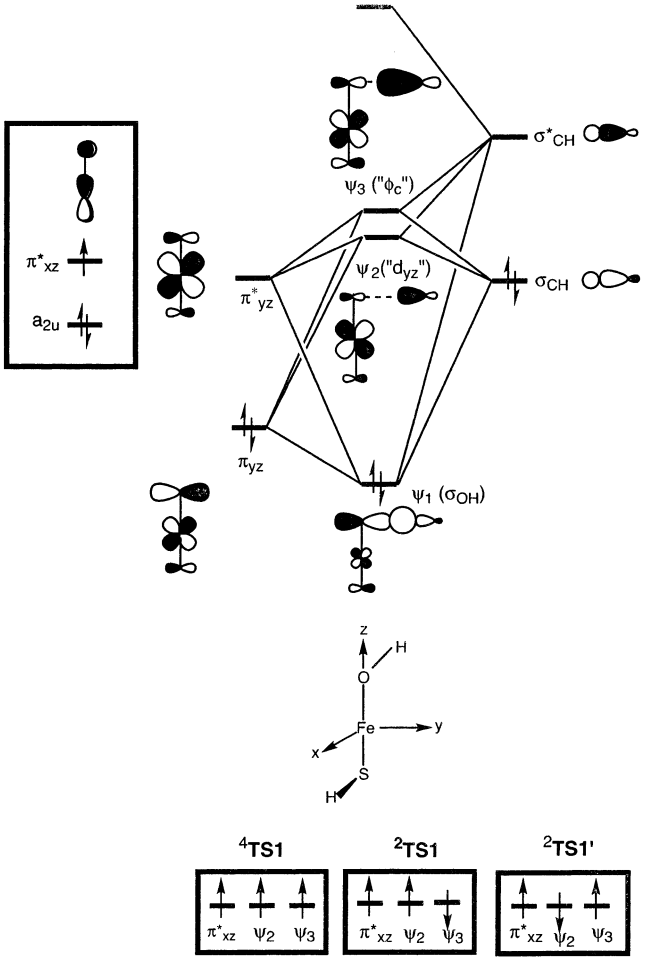

Figure 4. Schematic orbital interaction diagram depicting the orbital mixing in the hydrogen abstraction transition states.

The mixing of filled π_{yz} and π^*_{yz} with the σ and σ^* orbitals of the stretched C−H bond generates four orbitals of the TS. The lowest orbital is made from an initial bonding combination of π_{yz} and σ, to which π^*_{yz} and σ^* mix to increase the bonding interaction across the newly forming O- - -H bond. The result is an orbital, ψ_1 that has dominant σ_{OH} character. The second orbital is made from an initial antibonding combination of π_{yz} and σ, to which π^*_{yz} and σ^* mix to decrease the antibonding interaction across the O- - -H linkage. The resulting orbital, ψ_2, becomes virtually nonbonding with respect to the O- - -H interaction and carries significant d_{yz} and methyl contributions with a heavier d_{yz} character. The third orbital results from an initial bonding of π^*_{yz} and σ^*, to which π_{yz} and σ mix to reduce the bonding interaction across the O- - -H linkage. This orbital, ψ_3, also has significant d_{yz} and methyl contributions with a heavier methyl character, ϕ_C. The fourth orbital is completely antibonding and is not depicted in the diagram.

There are four electrons, initially residing in π_{yz} and σ_{CH}, which will occupy the orbitals of the transition state. The σ_{OH} orbital will always be doubly filled and need not be considered for the purpose of understanding the spin density distribution. The remaining two electrons will occupy the ψ_2("d_{yz}") and ψ_3("ϕ_C") orbitals, where the corresponding dominant characters are indicated in quotation marks. Since π^*_{xz} is singly occupied, the open-shell configuration for all the TS's will be $\pi^{*\,1}_{xz}$ ψ_2("d_{yz}")^1 ψ_3("ϕ_C")^1. Three electrons in three orbitals will give rise to three triradicaloid states, one HS quartet state and two LS doublet states.[33] This is the reason we observed only three TS's; **^{4}TS1**, **^{2}TS1**, and **^{2}TS1′**, even though there are initially four states of Cpd I(Ru). We note that since the orbitals ψ_2("d_{yz}") and ψ_3("ϕ_C") are both higher-lying than a_{2u}, even if our starting orbital population were of the $^{4,2}A_{2u}$ type, namely a_{2u}^1 $\pi^{*\,1}_{yz}$, in the final states the a_{2u} orbital would have still acquired double occupancy, leading thereby to the same open-shell configuration, $\pi^{*\,1}_{xz}$ ψ_2("d_{yz}")^1 ψ_3("ϕ_C")^1. Thus, the three TS's can be traced back to the composite states, $^{4,2}A_{2u}-{}^2\Pi_{xz,yz}$, of Cpd I(Ru).

Let us turn now to analyze the spin density distribution. In the HS **^{4}TS1**, all the singly occupied orbitals are with spin-up, and hence, the TS will have significant spin density on RuO and a positive spin density on the methyl group, as shown in Scheme 6. The two LS TS's differ by the two orbitals that occupy the spin-paired electrons, as shown at the bottom of Figure 4. Spin pairing of the electrons in ψ_2("d_{yz}") and ψ_3("ϕ_C") results in the lower-energy state, **^{2}TS1**. Since the $\pi^{*\,1}_{xz}\psi_2$("d_{yz}")^1 occupancy in this TS has both spins up, this results in a significant spin density on Ru, while the spin-down electron in ψ_3("ϕ_C")^1 results in a negative spin density on the methyl group. In contrast, spin-pairing of the electrons in ψ_2("d_{yz}") and π^*_{xz} generates the second doublet state, **^{2}TS1′** that is higher in energy relative to **^{2}TS1** because of the loss of exchange interactions on Ru (d_{yz} − d_{xz}). In this doublet state, **^{2}TS1′**, the spin density on Ru arises from contributions of two spin-opposing electrons in $\pi^{*\,1}_{xz}$ ψ_2("d_{yz}")^1, and hence the spin density on Ru is close to zero. The remaining spin-up electron in ψ_3("ϕ_C") contributes a positive spin density on the methyl group. As may be seen from Scheme 6, these spin density patterns predicted from the interaction diagram in Figure 4 are in perfect agreement with the computed spin densities. Thus, all the TS's possess the same open-shell configuration that corresponds approximately to a Ru^{IV} oxidation state.

The difference between Ru and Fe originates again in the relative energy level of the corresponding π^* orbitals. In Ru, this orbital is high, and therefore, the a_{2u} orbital is kept doubly occupied, while ψ_2("d_{xz}") becomes singly occupied. In Fe, where this orbital is low, the Fe^{III} state with single occupancy in a_{2u} and double occupancy in ψ_2("d_{xz}") becomes competitive in energy with the Fe^{IV} state, in which a_{2u} is doubly occupied, while ψ_2("d_{xz}") is singly occupied.

Another difference between ruthenium and iron comes from the geometric features of Cpd I(Ru) and Cpd I(Fe). The former has a long Ru−O bond, such that the reacting alkane keeps far away from the porphine and does not overlap significantly with the a_{2u} orbital. By contrast, in Cpd I(Fe) where the Fe−O bond is shorter, the reacting alkane is closer to the porphine ring, and hence, its orbitals can mix with the a_{2u} orbital. Thus, in Ru, the a_{2u} orbital is kept almost pure and doubly occupied by virtue of its relatively low energy (compared with the π^* orbitals) and due to the long Ru−O bond that prevents a significant overlap of a_{2u} with the orbitals of alkane.

Table 2. Solvent Effect on the Relative Energies[a] of the States of Cpd I(Ru) and the Hydrogen Abstraction Transition States

	Cpd I(Ru) states				hydrogen abstraction Ts's		
conditions[b]	$^4A_{2u}$	$^2A_{2u}$	$^2\Pi_{xz}$	$^2\Pi_{yz}$	**^{4}TS1**	**^{2}TS1**	**^{2}TS1′**
$\epsilon = 1$	0.00	−0.56	−5.14	−3.57	2.4	0.0	2.8
$\epsilon = 5.7$	0.00	−0.35	0.25	1.38	2.5	0.0	3.2
$\epsilon = 33.6$	0.00	0.16	3.57	1.49	2.5	0.0	3.4
$\epsilon = 80.4$	0.00	0.00	4.13	2.16	2.5	0.0	4.0

[a] In kcal/mol. [b] $\epsilon = 1$ refers to gas-phase conditions. $\epsilon = 5.7$, 33.6, and 80.4 correspond to the solvents: chlorobenzene, methanol, and water, respectively.

Solvent Effect on Reactants and Hydrogen Abstraction Transition States. Table 2 summarizes the effect of medium polarity on the energetics of the states of Cpd I(Ru) and on the three TS's for C−H bond activation. It is apparent that with medium polarization, the reactant state is almost quadruply degenerate, and reactivity must be considered as emanating from the entire composite of $^{4,2}A_{2u}$ and $^2\Pi_{xz,yz}$ states. This sensitivity of the states of Cpd I(Ru) originates in the chameleon behavior of the $^{4,2}A_{2u}$ states.[21] In contrast to the reactant states, the TS species are less sensitive to the choice of the solvent used. This lack of sensitivity of the TS's is in line with the double occupancy of the a_{2u} orbital. In this respect, in the iron case, both the reactant $^{4,2}A_{2u}$ states as well as the corresponding TS's exhibit sensitivity to medium polarization.[30c,d]

Mechanistic Features: Comparison of Ruthenium to Iron. Figure 5 shows the assembled energy profile for methane hydroxylation by Cpd I(Ru). It is seen that the mechanism involves two phases: a C−H bond activation phase and a C−O rebound phase. As shown in Figures 2 and 3 above, all the TS's of the first phase have the appearance and properties of hydrogen abstraction species. However, while the HS mechanism is indeed stepwise with a long-lived carbon-radical intermediate, the LS mechanisms are effectively concerted once the rebound position is achieved. This multistate reactivity is similar to the situation in alkane hydroxylation by Cpd I(Fe).[23a,b,30a,c,d,31c] However, a closer look reveals significant differences.

First, the lowest hydrogen abstraction barrier in Figure 5 is 22.9 kcal/mol (measured relative to the $^2\Pi_{xz}$ state of Cpd I(Ru)), whereas the corresponding barrier in the Cpd I(Fe) case is 26.5 kcal/mol.[23a] In this sense, even though methane is a very poor donor, still the calculations reproduce the experimental results that imply higher electrophilicity of the ruthenium−oxo catalysts compared with that of the iron−oxo catalysts.[22]

A second difference concerns the rebound process for the HS mechanism. The rebound barrier in Figure 5 is 11.9 kcal/mol compared with only 4.7 kcal/mol for the iron species.[23a] As already argued above,[23a] the rebound barrier originates in the electronic promotion, which attends the C−O bond formation and which transpires from the methyl orbital, ϕ_C, to the metal $d_{z^2}(\sigma^*)$ orbital (Scheme 5). The $d_{z^2}(\sigma^*)$ orbital involves a metal−oxygen antibonding interaction (see Scheme 2), and since the 4d(Ru)−2p(O) overlap is stronger than 3d(Fe)−2p(O) overlap,[21] the $d_{z^2}(\sigma^*)$ orbital of ruthenium is expected to be higher than the $d_{z^2}(\sigma^*)$ of iron. Indeed, as revealed by the data

(33) Pilar, F. L. *Elementary Quantum Chemistry*; McGraw-Hill Book Co.: Singapore, 1990.

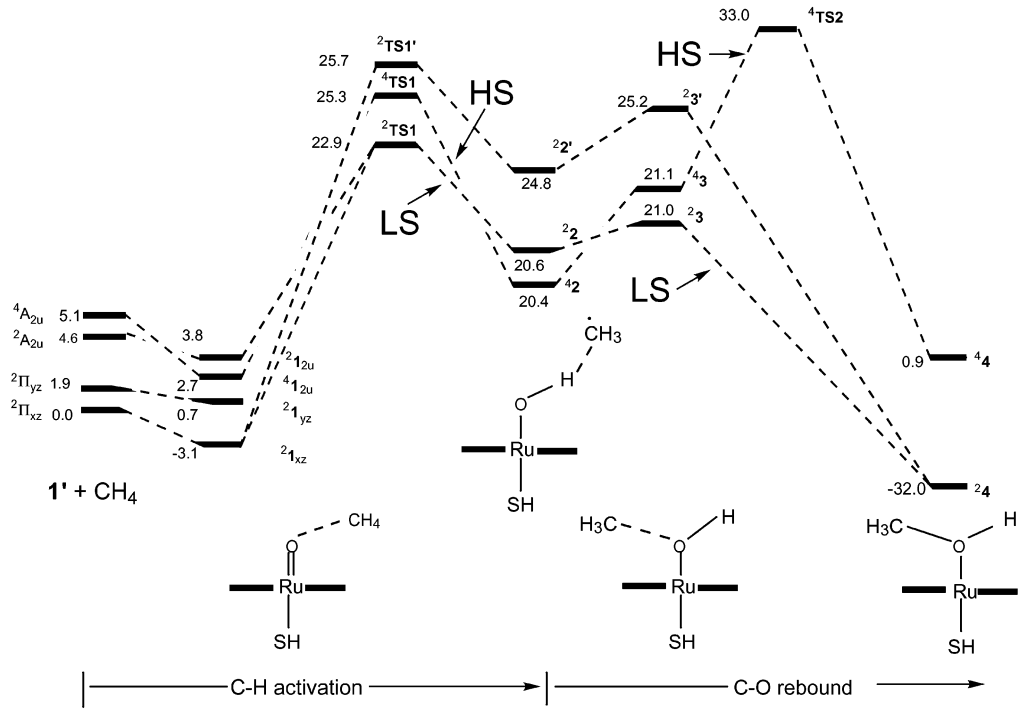

Figure 5. Energy profiles (values in kcal/mol) of the methane hydroxylation reaction by Cpd I(Ru).

Scheme 7. Comparison of the Orbital Energy Gaps (kcal/mol) Relevant to the Rebound and Suicidal Heme-Alkylation Processes That Are Nascent from the Intermediates for Fe and Ru

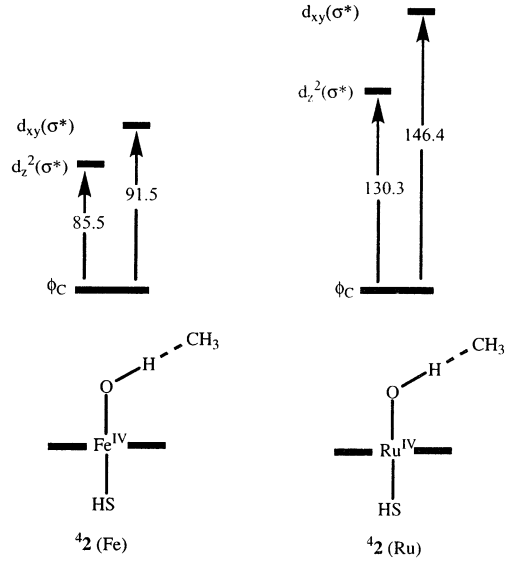

in Scheme 7, the ϕ_C- $d_{z^2}(\sigma^*)$ orbital energy gap is much larger for ruthenium compared to iron. Since this orbital energy gap determines the height of the rebound barrier, consequently, the corresponding barrier in the ruthenium case becomes much larger compared with that in the iron case.

With such a high rebound barrier on the HS ruthenium mechanism, the total barrier for the HS hydroxylation becomes 33.0 kcal/mol, compared with 22.9 for the LS rebound. Under conditions of fast spin crossover, the dominant pathway will be the LS one, and hence, alkane hydroxylation by Cpd I(Ru) will be more stereoselective compared with the reaction with Cpd I(Fe). If however, spin crossover is slow, a small percentage of HS trajectories will manifest, but again, the high rebound barrier will limit this. Thus, in any scenario, a higher stereoselectivity is expected for the ruthenium−oxo catalyst compared to that for the iron−oxo catalyst. Furthermore, for axial ligands that are much poorer donors than the thiolate, the $^4A_{2u}$ state will be high-lying,[29] and ^{2}**TS1** will dominate the hydroxylation pathway.

A related aspect is the suicidal reaction[34] that is often observed in the iron−oxo catalysts, and which leads to heme alkylation. As shown by us before,[35] the suicidal complex can originate from the intermediate ^{4}**2** by electron promotion from the alkyl orbital ϕ_C (Scheme 5) to the $d_{xy}(\sigma^*)$ orbital. In the case of iron, where the $d_{xy}(\sigma^*)$ orbital is not too high, the suicidal reaction was found to have a moderate reaction barrier (ca. 10 kcal/mol). However, in the case of ruthenium, where the $d_{xy}(\sigma^*)$ orbital is expected to be higher, the barrier for the suicidal reaction will also be high. A comparison of the relevant ϕ_C−$d_{xy}(\sigma^*)$ orbital energy gaps for ^{4}**2**(Ru^{IV}) vis-á-vis ^{4}**2**(Fe^{IV}) in Scheme 7 shows that it is indeed the case. As such, suicidal side products for ruthenium−oxo catalysts will require a much higher barrier than in the iron case and are therefore less likely. All in all, therefore, *our results suggest that ruthenium−oxo catalysts should be more robust than their iron−oxo analogues*.

Conclusions

The preceding results and discussion show that (HS)PorRuO systems can indeed act as efficient hydroxylation catalysts. Since both the reactants in the doublet state, viz., ^{2}**1**$_{2u}$ (Ru^{IV}) and ^{2}**1**$_{xz}$ (Ru^{V}), pass through the same set of hydrogen abstraction transition states, leading to Ru^{IV} intermediates, we can say that (HS)PorRuO, in both $Ru^{IV}Por^{\bullet+}$ and Ru^{V}Por oxidation states are capable of acting as catalysts. However, for ligands that are

(34) See, for example: Ortiz de Montellano, P. R.; Beilan, H. S.; Kunze, K. L.; Mico, B. A. *J. Biol. Chem.* **1981**, *256*, 4395−4399; Kunze, K. L.; Mangold, B. L.; Wheeler, C.; Beilan, H. S.; Ortiz de Montellano, P. R. *J. Biol. Chem.* **1983**, *258*, 4202−4207.
(35) de Visser, S. P.; Ogliaro, F.; Shaik, S. *Angew. Chem., Int. Ed.* **2001**, *40*, 2871−2874.

poorer donors than HS^-, the reactivity will be dominated by the Ru^V species, as inferred experimentally.[1a, 22]

In general, the Ru−oxo catalysts appear to be more robust than the iron−oxo analogues. Unlike the iron catalyst, here the hydroxylation reaction is expected to follow largely a single-state reactivity with a dampened high-spin reactivity due to the very large barrier at the rebound step. Thus, the reactions of the ruthenium−oxo catalyst are expected to be more stereoselective than the corresponding iron−oxo reactions. The ruthenium catalyst is expected to produce also fewer suicidal side products[34] that involve heme alkylation. In addition, our computations reveal lower hydrogen abstraction barriers for the ruthenium complex compared with those for the iron case.

These reactivity features of the ruthenium−oxo originate from two fundamental factors. One is the strong 4d(Ru)−2p(O) overlap (also 4d(Ru)−2p(N)), which produces low-lying π(Ru−O) orbitals and high-lying π*(Ru−O), σ*(Ru−O), and σ*(Ru−N) orbitals. The high-lying π* orbitals result in an inherent preference of ruthenium for higher-valent oxidation states with closed-shell porphyrin macrocycle, in contrast to iron, which prefers lower oxidation states with open-shell porphyrin. The high-lying σ*(Ru−O) orbital raises the rebound barrier on the HS surface and practically inactivates the HS state reactivity, while the high-lying σ*(Ru−N) orbital minimizes the suicidal products.[35] The second factor is the longer Ru−O distance (compared with Fe−O) that prevents any significant overlap of the alkane with the porphyrin orbitals. The preference for the LS reactivity may be further augmented due to the expected higher efficiency of spin crossover in the ruthenium complex versus that in the iron analogue. An eventual synthesis of stable $PorRu^VO$ model compounds[1a] is expected to elucidate the relative properties of iron and ruthenium catalysts. Reconstitution of a P450 isozyme or a similar enzyme with an Fe ⟹ Ru replacement, if ever successful,[36] is likely to lead to a direct comparison of the two Cpd I species on equal footing.

Acknowledgment. We acknowledge the financial support from the Israel Science Foundation and the Ministry of Science, Culture and Sport. We are thankful to Professor J. T. Groves for useful discussions and for sharing unpublished results (see ref 22). This paper is dedicated to Professor Björn Roos on the occasion of his 65th birthday.

Supporting Information Available: Eight tables with the geometric and other properties (PDF). This material is available free of charge via the Internet at http://pubs.acs.org.

JA0282487

(36) As remarked by a reviewer, functionalized porphyrins, particularly with thiolate coordination, have difficulties to survive the harsh conditions of inserting Ru in place of Fe.